Modeling Unidirectional Composite Laminates Using XFEM

Andrew W. Hulton
Ranges, Engineering, and Analysis Department

NEWPORT

Naval Undersea Warfare Center Division
Newport, Rhode Island

PREFACE

This report was funded under NUWC Division Newport Internal Investment Program, NWA 300000089394/0010. The principal investigator was Andrew W. Hulton (Code 7023).

The technical reviewer was Matthew E. Johnson (Code 7023).

Reviewed and Approved: 30 June 2015

Eric S S pigel

Eric S. Spigel
Head, Ranges, Engineering, and Analysis Department

REPORT DOCUMENTATION PAGE

The public reporting burden for this collection of information is estimated to average 1 hour per response, including the time for reviewing instructions, searching existing data sources, gathering and maintaining the data needed, and completing and reviewing the collection of information. Send comments regarding this burden estimate or any other aspect of this collection of information, including suggestions for reducing this burden, to Department of Defense, Washington Headquarters Services, Directorate for Information Operations and Reports (0704-0188), 1215 Jefferson Davis Highway, Suite 1204, Arlington, VA 22202-4302. Respondents should be aware that notwithstanding any other provision of law, no person shall be subject to any penalty for failing to comply with a collection of information if it does not display a currently valid OPM control number.
PLEASE DO NOT RETURN YOUR FORM TO THE ABOVE ADDRESS.

1. REPORT DATE (DD-MM-YY) 30-06-2015	2. REPORT TYPE Technical Report	3. DATES COVERED (From – To)

4. TITLE AND SUBTITLE	5a. CONTRACT NUMBER
Modeling Unidirectional Composite Laminates Using XFEM	5b. GRANT NUMBER
	5c. PROGRAM ELEMENT NUMBER
6. AUTHOR(S)	5.d PROJECT NUMBER
Andrew W. Hulton	5e. TASK NUMBER
	5f. WORK UNIT NUMBER

7. PERFORMING ORGANIZATION NAME(S) AND ADDRESS(ES)	8. PERFORMING ORGANIZATION REPORT NUMBER
Naval Undersea Warfare Center Division 1176 Howell Street Newport, RI 02841-1708	TR 12,178

9. SPONSORING/MONITORING AGENCY NAME(S) AND ADDRESS(ES)	10. SPONSORING/MONITOR'S ACRONYM
Naval Undersea Warfare Center Division 1176 Howell Street Newport, RI 02841-1708	NUWC
	11. SPONSORING/MONITORING REPORT NUMBER

12. DISTRIBUTION/AVAILABILITY STATEMENT

Approved for public release; distribution is unlimited.

13. SUPPLEMENTARY NOTES

14. ABSTRACT

Fiber-reinforced polymers (FRPs)—composites consisting of a thermoset or thermoplastic polymer matrix reinforced by carbon, glass, or aramid fibers—have been used as a substitute for more conventional materials in a wide range of applications, particularly in the aerospace, defense, and automobile industries. FRP strength-to-weight ratio and load-carrying capacity and toughness are superior to those of typical metals. Because of the widespread availability of measurement techniques, experimental testing of composite materials has largely outpaced the computational modeling ability of such complicated materials, forcing design of composite structures to follow a build-test-build cycle. The use of the extended finite-element method (XFEM) has revolutionized the design process: it improves modeling efficiency and allows investigation of failure mechanisms.

The research documented in this report clearly demonstrates that the design of composite structures is no longer restricted by the time-consuming and costly build-test-build methodology. Specifically, this research demonstrates the ability of XFEM, combined with cohesive behavior, to model various modes of failure in composite materials simultaneously. These advancements in computational physics-based modeling are changing the manufacture of FRPs: comprehensive modeling techniques can significantly reduce the effort required to build and test future composite structures and will allow previously untested composite arrangements to be properly analyzed prior to any physical testing, vastly reducing cost and time requirements.

15. SUBJECT TERMS

Undersea Warfare	Fiber-Reinforced Composites	Finite-Element Method	Fracture Mechanics	Physics-Based Modeling
Cohesive Interface	Extended Finite-Element Method	Linear Elastic Fracture Mechanics	Virtual Crack Closure Technique	

16. SECURITY CLASSIFICATION OF:			17. LIMITATION OF ABSTRACT	18. NUMBER OF PAGES	19a. NAME OF RESPONSIBLE PERSON
a. REPORT Unclassified	b. ABSTRACT Unclassified	c. THIS PAGE Unclassified	SAR	27	Andrew W. Hulton
					19b. TELEPHONE NUMBER (Include area code) 401-832-6830

TABLE OF CONTENTS

Page

LIST OF ILLUSTRATIONS

Figure   **Page**

LIST OF TABLES

LIST OF ABBREVIATIONS AND ACRONYMS

3-D	Three-dimensional
BK	Benzeggagh-Kenane
CFRP	Carbon-fiber-reinforced polymer
CZM	Cohesive zone method
DCB	Double cantilever beam
ECT	Edge crack torsion
ENF	End-notched flexure
FEM	Finite-element method
FRP	Fiber-reinforced polymer
GPa	Gigapascal
ksi	Kilopound per square inch
LEFM	Linear elastic fracture mechanics
MMB	Mixed-mode bending
MPa	Megapascal
msi	megapound per square inch
N	Newton
Pa	Pascal
PBM	Physics-based modeling
PUM	Partition-of-unity method
UD	Unidirectional
VCCT	Virtual crack closure technique
XFEM	Extended finite-element method

LIST OF SYMBOLS

D	Scalar cohesive damage variable
E	Young's modulus of elasticity
G	Shear modulus of elasticity
G_C	Critical material strain energy release rate
G_I (G_{II}, G_{III})	Mode strain energy release rate
G_{IC} (G_{IIC}, G_{IIIC})	Critical Mode strain energy release rate
G_{IC} (G_{IIC}, G_{IIIC})	Critical Mode strain energy release rate
G_T	Total strain energy release rate
H	Heaviside function
p_e	External pressure on cylinder
q_J^0	Enrichment coefficients
S_C	Set of elements encompassing crack
S_H	Set of elements encompassing crack tip
$t_n(t_s,\ t_t)$	Normal and tangential cohesive stress
$t_n^0(t_s^0,\ t_t^0)$	Normal and tangential cohesive stress at failure
u_I	Nodal degrees of freedom
$\delta_n(\delta_s,\ \delta_t)$	Normal and tangential cohesive separation
$\delta_n^0(\delta_s^0,\ \delta_t^0)$	Normal and tangential cohesive separation at failure initiation
$\delta_n^f(\delta_s^f,\ \delta_t^f)$	Normal and tangential cohesive separation at final failure
σ_{ps}	Principal stress
σ_{ps}^f	Fiber principal stress at failure
σ_{ps}^m	Matrix principal stress at failure
σ_y	Material yield stress
v	Poisson's ratio
$\Psi^{(j)}$	Enrichment coefficients near crack tip

MODELING UNIDIRECTIONAL COMPOSITE LAMINATES USING XFEM

INTRODUCTION

Fiber-reinforced polymers (FRPs)—composites consisting of a thermoset or thermoplastic polymer matrix reinforced by carbon, glass, or aramid fibers—have the potential to dramatically influence the design and manufacturing processes of innumerable industries. The significance of FRP composites is that they can be customized in the manufacturing process to meet the needs of specific applications. For example, FRPs are rapidly becoming the preferred material of construction for applications that require a superior strength-to-weight ratio and a high load-carrying capacity. FRPs are of particular interest to the U.S. Navy because of their potential use in underwater applications where corrosion-resistance, weight, and implosion-resistance are indispensable design factors.

Because of the widespread availability of measurement techniques, experimental testing of composite materials has largely outpaced the computational modeling ability of such complicated materials—thus, relegating the design of composite structures to a build-test-build methodology. Recent advancements in computational physics-based modeling (PBM), however, are changing the manufacture of FRPs: comprehensive modeling techniques can significantly reduce the effort required to build and test future composite structures and will allow previously untested composite arrangements to be properly analyzed prior to any physical testing, vastly reducing cost and time requirements.

The finite-element method (FEM) has been a popular computational analysis technique for modeling mechanical deformations and failure for any material, including FRPs. Numerical computation of FRP fracture has historically consisted of imposing failure conditions on a homogenous material with averaged composite properties to capture one of the common failure methods, such as delamination. Recent research has investigated fracture using the extended finite-element method (XFEM). Initiation and propagation of multiple cracks can be modeled simultaneously without mesh refinement or successive re-meshing near the crack tip. Crack propagation is modeled using the virtual crack closure technique (VCCT) that is typically applied to linear elastic fracture mechanics (LEFM).

This report documents a three-dimensional (3-D) computational model of a portion of a carbon fiber/epoxy composite cylinder, incorporating both cohesive interface failure as well as the XFEM capability available in Abaqus v6.13. A traction-separation cohesive failure model is used to evaluate failure in the fiber/matrix interface. XFEM is used to model crack growth and propagation throughout the fibers and matrix. The cylinder segment is loaded under external pressure to simulate implosion due to hydrostatic depth pressure. Rather than modeling the composite as a single material (for example, homogenization), individual groups of fibers are modeled within a distinct matrix material. The composite consists of either one layer of unidirectional (UD) carbon fibers or two layers with 0°/90° fiber orientation. Three groups of

fibers are modeled for each layer. The combination of both cohesive interface failure and material failure using XFEM in one model allows the cohesive failure and fracture thresholds to be determined for given inputs. These inputs may include resin and fiber material, volume fraction, fiber layup, interfacial cohesive strength, and material fracture toughness. Analyses with varying input parameters are presented to highlight critical thresholds for the given geometry and loading condition.

With the information presented in this report, future composite structures can be analyzed with multiple methods of failure investigated simultaneously. Using previously obtained composite material properties, thorough modeling of future designs can save significant time and effort in experimentally testing and modifying composite constructions.

HISTORICAL DEVELOPMENTS IN FRP COMPOSITE EVALUATION

EXPERIMENTAL TESTING

FRP composites consist of a thermoset or thermoplastic polymer matrix reinforced by carbon, glass, or aramid fibers. While individual fibers have diameters around 5 to 10 μm, thousands of fibers are typically bundled together to form a tow. Single-direction-fiber-tow layers can be (1) stacked into varying orientation plies or (2) they can be woven together. The nature of manufacturing FRPs provides a unique ability to customize the FRP for specific applications. Fiber and matrix material selection, fiber/matrix volume fraction, and laminate organization are just a few of the many factors associated with designing and manufacturing a desired composite material.

Although numerous options exist when the use and design of FRP composites are being contemplated, the exact mechanical nature of the composite has not been fully evaluated. Typical research of composite materials has consisted of extensive testing of previously built structures. For example, composite cylinders designed for underwater applications are first subjected to rigorous impact and implosion testing to determine their structural efficacy.[1, 2] Tarpani et al.[3] determined quasi-static and impact properties of various aeronautical-grade carbon/epoxy laminate structures to quantify the strength of various composite constructions.

Furthermore, the effects of different loading scenarios are not well understood. Although FRPs show particularly good material properties in the fiber axial direction, transverse loads on complex structures can lead to failure at lower stress states. The failure of FRPs under compression, which leads to the creation of fiber kink bands, was experimentally studied by Kyriakides et al.[4]. Other factors, such as sensitivity to rate of deformation, can be measured for various composite combinations.[5, 6] Kepple et al.[7] showed that novel composite organizations, such as carbon nanotubes grown onto woven carbon fiber composites, can be created to combat the shortfalls of traditional composite structures.

2

FRP FAILURE METHODS

Much work has been done to attempt to comprehensively analyze and model the constituents of a composite material. FRPs fail by one or more of four different methods: (1) fiber fracture, (2) matrix cracking, (3) delamination, or (4) fiber pull-out. The most common causes of these failure methods are the failure of the matrix (matrix cracking, delamination) or the failure of the fiber/matrix interface (fiber pull-out, delamination). Each failure phenomenon corresponds to a failure in one of three primary modes of material fracture: crack opening, in-plane shearing, or out-of-plane tearing. A review of the various modes of fracture, which are discussed in the next section, is provided by Prasad et al.[8] A comprehensive overview of the mathematical modeling of different fracture phenomena in fiber composites is provided by Mishnaevsky and Brøndsted.[9] In addition, Pinho et al.[10] developed physically based criteria for calculating multiple modes of failure in FRPs.

These composite structures consist of complex material interactions and can be analyzed at differently sized scales. The majority of research has focused on investigating composites in a large scale, where the composite is assumed to be a homogenous material with averaged mechanical properties. Other research has focused on the random nature of individual fibers in the microscopic scale.[9, 11]

Fracture of composite laminates has been modeled using a variety of FEMs. Krueger[12] documented a large review of fracture toughness characterization for multiple modes of fracture using the VCCT. Sun et al.[13] developed an FEM using plate elements to characterize fracture toughness in woven carbon/epoxy composites under mixed-mode loading. Waseem and Kumar[14] investigated delamination of carbon fiber/epoxy composites using multiple fracture techniques. Camanho et al.[15] used interfacial decohesion elements between layers to model delamination. Delamination of materials has also been studied by Zhao,[16] who focused on the viscoelastic behavior of composites under elevated temperature. Wimmer et al.[17] analyzed onset and growth of cracks in laminated composites in curved structures. With rigorous modeling efforts, certain capabilities of existing material constructions can be improved upon. Segala and Cavallaro[18] investigated the failure modes of UD fibrous composites subjected to ballistic impacts in an effort to increase energy absorption capacities.

While most of the research on the fracture of composite materials has used conventional FEM techniques, the XFEM provides unique capabilities in modeling fracture. Though standard finite-element analyses require a highly refined mesh near the assumed crack location, XFEM allows cracks to form and propagate along a natural crack path without prior knowledge of its location. In addition, continual re-meshing near the crack front is not required. Eliminating these computationally expensive methods makes modeling fracture using XFEM markedly easier. Widespread research has been conducted implementing XFEM into established finite-element codes. Recently, commercial software packages such as Abaqus have included an XFEM capability. With these new abilities, previously impractical simulations involving composite structures can be analyzed quickly and efficiently.

Primarily, XFEM can be used to validate experimental procedures and predict future test results. Motamedi and Milani[19] developed a 3-D model utilizing XFEM and the cohesive zone method (CZM) to analyze delamination under mode I loading (modes I, II, and III are discussed in the Fracture Mechanics section). Levén and Rickert[20] investigated the integrity of modeling various cracks using XFEM. Grogan et al.[21] used an XFEM-based methodology to validate mode I and II fracture when analyzing thermal fatigue of carbon-fiber-reinforced polymers (CFRP).

With the XFEM, a wide range of composite materials can be evaluated. For example, Benvenuti et al.[22] applied XFEM concepts to modeling FRP-reinforced concrete and Sosa and Karapurath[23] used XFEM to model delamination of fiber-metal laminate composites with orthotropic material properties. Moreno et al.[24] modeled and analyzed crack propagation in chopped glass-fiber composites under biaxial loading and compared the results to experimental findings. Motamedi[25] investigated the nonuniform nature of composites using a combination of XFEM and other commercial FEM software. Instead of using typical isotropic material properties, Nagashima and Suemasu[26] developed an orthotropic material model undergoing mode I delamination.

MODELING INTERFACE INTERACTIONS BETWEEN DISTINCT FIBER GROUPS AND THE MATRIX

Although extensive research has been conducted in modeling FRPs using finite-element techniques at both micro (individual fibers) and macro (homogenous composite materials) scales, little work has been done to model interface interactions between distinct fiber groups and the matrix in conjunction with matrix fracture using XFEM. A goal of this research effort was to develop a three-dimensional (3-D) finite-element model that incorporated multiple failure techniques available in Abaqus v6.13. This research focused on separating individual tows of fibers from the surrounding matrix. Distinct cylindrical groups of fibers were treated as a homogenous material with a smooth interface with the surrounding matrix. By defining the model in this way, interfacial cohesion could be implemented while the overall cylindrical geometry was maintained. In addition to evaluating cohesive interface failure between the fibers and matrix, this research also evaluated matrix/fiber fracture using the XFEM.

The developed model was used to study the onset of cracking and decohesion in unidirectional one- and two-ply carbon-fiber/epoxy composite cylinders. The loading condition on the composite cylinder was exterior hydrostatic pressure—a particularly useful loading condition because of its widespread effect on a variety of underwater systems. Compression caused by external pressure results in material fracture and eventual implosion, presenting a significant concern for designers.

4

FRACTURE MECHANICS

In a generic material, three different modes of fracture can occur (see figure 1):

1. Mode I fracture results in two crack faces being pulled away from each other.

2. Mode II fracture occurs because of in-plane shear loading, where the two fractured surfaces slide with respect to each other along the crack plane.

3. Mode III fracture, out-of-plane shear due to shear loading, occurs when the crack faces separate out of the crack plane.

The three failure modes illustrated in figure 1 correspond to the various modes of failure in FRPs previously mentioned: fiber fracture, matrix cracking, delamination, or fiber pull-out. Delamination is the result of a mode I fracture where separate layers of a composite are torn away. Fiber fracture and matrix cracking are typically a function of mode II or III fractures where the material undergoes shear failure. Fiber pull-out happens when the cohesive interface between the fiber and matrix severs, allowing the fiber to slide through the matrix.
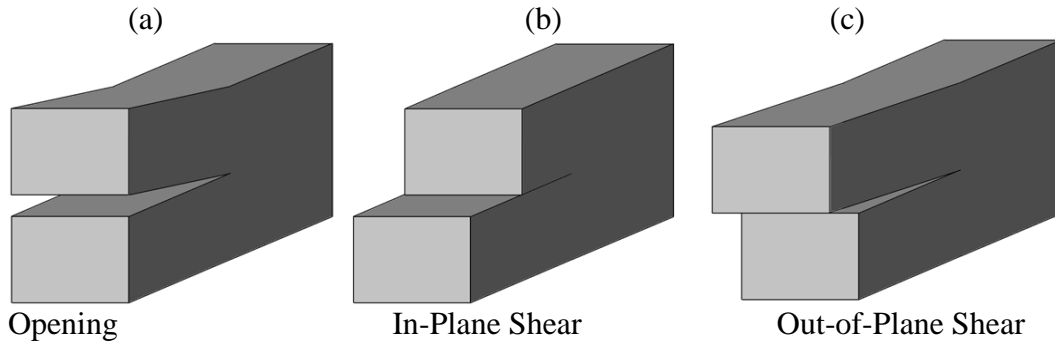
(a) (b) (c)

Opening   In-Plane Shear   Out-of-Plane Shear
Figure 1. (a) Mode I, (b) Mode II, (c) Mode III Fracture

The onset and growth of failure can be determined by comparing the strain energy release rate G_T to a critical fracture toughness value G_C. G_C is an experimentally determined material property and can be broken down into a combination of the individual mode fracture toughness values G_{IC}, G_{IIC}, and G_{IIIC}. G_T is a summation of G_I, G_{II}, and G_{III}, which correspond to energy release rates due to mode I, II, and III fractures, respectively. When $G_T > G_C$, the crack can be expected to propagate. Using these individual strain energy release rates, an overall failure criterion can be established. Benzeggagh and Kenane created a simple mathematical relationship combining the various mode strain energy release rates to determine G_C, which is shown in equation (1):

$$G_C = G_{IC} + (G_{IIC} + G_{IIIC} - G_{IC})\left(\frac{G_{II} + G_{III}}{G_T}\right)^m$$

$$G_T = G_I + G_{II} + G_{III}. \tag{1}$$

Typically, mode I fracture toughness G_{IC} is determined through the double cantilever beam (DCB) test.[6, 28] One end of a cantilever beam is pulled in opposite directions, splitting the beam in two. One of the most common experimental methods to measure mode II fracture toughness G_{IIC} is the end-notched-flexure (ENF) test. The test places a pre-cracked specimen into a three-point bending fixture. The crack, located at the end of the specimen, propagates along the length of the beam, resulting in delamination. A number of experiments have been proposed to measure mode III fracture energy release rate G_{IIIC}. One such method, described by Lee,[29] used the edge-crack-torsion (ECT) technique to investigate edge delaminations.

The vast majority of loading conditions on composite materials, however, involve mixed-mode loading. The mixed-mode-bending (MMB) test has been designed to encapsulate both modes I and II fracture simultaneously. The distance of the lever arm can be modified to provide loading that corresponds to a spectrum between pure mode I loading to pure mode II loading. An example of the mixed-mode bending is given by Prasad et al.[8]

XFEM

The XFEM was originally developed by Belytschko and Black[30] and is based on the partition-of-unity method (PUM) developed by Melenk and Babuška.[31] In PUM, additional enrichment functions are inserted into the conventional shape functions to account for discontinuities across the crack front. This continuity allows cracks to form and propagate without prior knowledge of the crack location and does not require remeshing throughout the simulation to maintain a fine mesh near the crack tip. The partition of unity is further described in detail by Belytschko et al.[32] The applied enrichment functions introduce additional degrees of freedom to affected elements, allowing the element to undergo transformation while maintaining continuity. In fracture mechanics, the enrichment functions consist of a near-tip asymptotic function, which captures the stress singularity at the crack tip, and a discontinuous function to map the displacement of the crack faces within an element. The enriched shape function[32] is given in equation (2):

$$u^h(x) = \sum_{\forall I} N_I(x) u_I + \sum_{J \in S_H} N_J(x) \left[H(f(x)) - H\left(f(x_J) \right) \right] q_J^0$$

$$+ \sum_j \sum_{K \in S_C} N_K(x) \left[\Psi^{(j)}(x) - \Psi^{(j)}(x_K) \right] q_K^{(j)\Psi^{(j)}}. \qquad (2)$$

The first summation includes the standard shape functions and nodal degrees of freedom, where N_I are the standard shape functions and u_I are nodal degrees of freedom. The second summation adds additional enrichments to the elements in the set S_H encompassing the crack tip. H is the Heaviside function and q_J^0 are enrichment coefficients. The third summation adds enrichments to the elements cut by the crack, excluding the elements inherent in the second term and are included in the set S_C. The term $\Psi^{(j)}$ is a set of enrichment functions near the crack tip. H is defined in equation (3) as:

$$H(f) = \begin{cases} 1, & f > 0 \\ 0, & \text{otherwise} \end{cases}. \qquad (3)$$

Because the crack affects only elements through which it passes, only the connecting nodes gain the additional degrees of freedom. Figure 2 shows a schematic of how the nodes are assigned around a given crack.
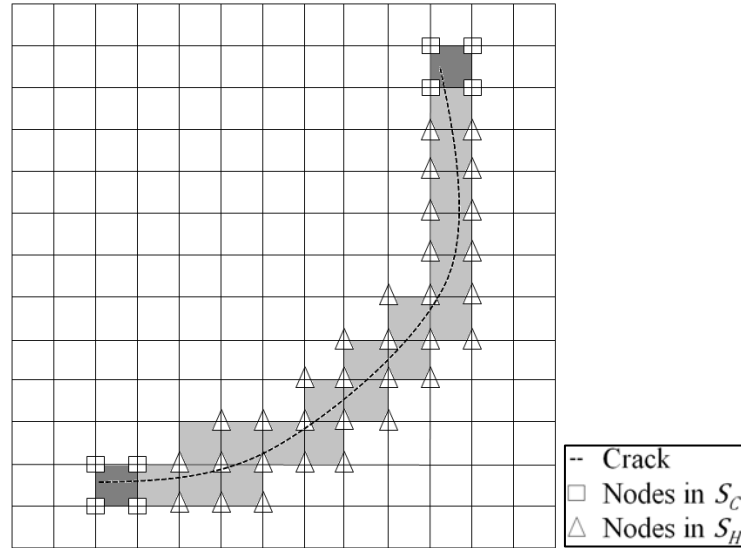

Figure 2. Crack Running Through a Set of Elements with Enriched Functions

Material Fracture

In Abaqus, two predominant methods can be used to calculate the movement of a crack through a material: one method is based on the cohesive traction-separation interaction, and the other is based on LEFM. Because the purpose of this research was to investigate fracture of a brittle composite matrix, LEFM was the chosen failure method. The stress energy release rates were determined using the VCCT. In VCCT, the energy absorbed through material fracture is assumed to be the work required to close the crack faces. Crack initiation occurs when the prescribed maximum principal stress σ_{ps} is reached. Upon initiation and growth, the crack follows the normal of the maximum tangential stress direction. The fracture energy release rate is calculated using the Benzeggagh-Kenane (BK) law.[27] The mode fracture toughness values can be calculated experimentally and used as inputs in the finite-element model. Table 1 lists a set of material properties typically seen in fiber/epoxy composites.[25]

Table 1. Material Properties for Common Fibers and Epoxy Matrix[25]

Property	*E* msi (GPa)	*v*	σ_y ksi (MPa)
Carbon Fiber	15-60 (103-414)	0.33	250-350 (1723-2413)
Glass Fiber	10-12 (69-83)	0.33	500-650 (3450-4480)
Kevlar (Aramid)	12-19 (83-131)	0.3	406 (2800)
Epoxy Matrix	0.35-0.7 (2.4-4.8)	0.28	7-15 (48-103)

COHESIVE INTERFACE

In addition to matrix fracture, this research also investigated the separation of the fiber/matrix interface, another method of failure. This separation occurs when shear or normal stresses overcome the interfacial bond, resulting in the fiber sliding through the matrix surface. In Abaqus, cohesion can be modeled between two surfaces in contact. Cohesive surfaces are assumed to be thin films with zero thickness that form a rigid bond. To break the cohesive bond, a damage criterion must be met. Prior to damage initiation, the two surfaces (fiber and matrix) possess a cohesive stiffness in each direction. These stiffness values, K_n, K_s, and K_t, represent a linear relationship between the cohesive stress $t_n(t_s, t_t)$ and cohesive separation $\delta_n(\delta_s, \delta_t)$ for the normal and shear directions. The damage criterion used in this model uses the maximum nominal stress in either the normal or shear directions, shown in equation (4):

$$\max\left\{\frac{\langle t_n \rangle}{t_n^0}, \frac{t_s}{t_s^0}, \frac{t_t}{t_t^0}\right\} = 1, \tag{4}$$

where t_n^0, t_s^0, or t_t^0 are the material input maximum nominal stresses in the normal and shear directions, respectively. Upon reaching the prescribed maximum stress $t_n^0(t_s^0, t_t^0)$, it is assumed that damage has occurred in the cohesive bond. After damage initiation has occurred, the cohesive interface follows a linear damage law until reaching the final displacement $\delta_n^f(\delta_s^f, \delta_t^f)$. Figure 3 shows the damage initiation and evolution path.
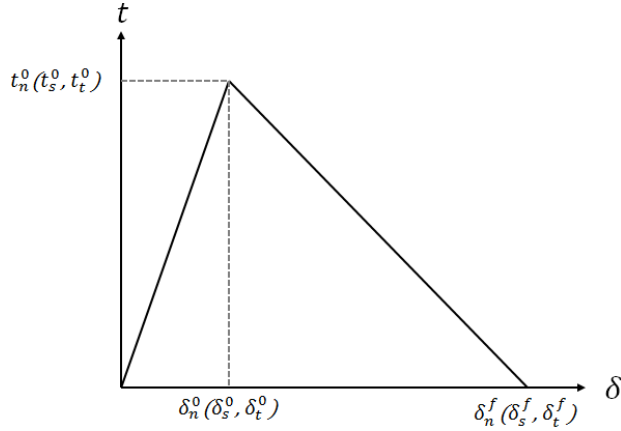

Figure 3. Interfacial Cohesive Behavior

The overall damage in the linear damage law is defined by the scalar variable D. When D reaches a value of 1, the bond is assumed to be completely severed. The nominal stress components are associated with D as:

$$t_n = \begin{cases} (1-D)\bar{t}_n, & \bar{t}_n \geq 0 \\ \bar{t}_n, & \text{otherwise} \end{cases}$$
$$t_s = (1-D)\bar{t}_s$$
$$t_t = (1-D)\bar{t}_t. \tag{5}$$

3-D FINITE-ELEMENT MODEL

DESCRIPTION

In this analysis, a cylindrical geometry was chosen because of its widespread use as an underwater vessel. Because of the symmetrical nature of cylinders, only a slice of the cylinder was required to be modeled; therefore, 1/20th of the cylinder circumference was used as a unit cell of the entire cylinder within a cylindrical coordinate system. Symmetry boundary conditions were imposed on the θ- and axial z-directions to both the fiber and matrix. With these dimensions, three fiber groups, or tows, with a diameter of 0.02 inch (0.5 mm) were modeled for each layer, with a 0.02-inch separation between the fibers. The two layers were oriented in the 0°/90° directions, with 0° corresponding to the cylinder axis and 90° in the circumferential θ-direction.

This orientation was chosen to highlight the differences in stress and fracture in the cylinder warp and weft directions. The cylinder wall thickness was 0.08 inch (2 mm), allowing 0.01 inch (0.25 mm) of matrix between the top and bottom plies. The selected geometry was chosen to accentuate the matrix filling between individual carbon fiber groups, allowing cracks to form and propagate throughout the matrix. In addition to having two layers of fibers, single-ply composites with fibers in the axial z-direction were analyzed separately. The purpose of analyzing single-ply composites was to isolate the potential damage mechanisms in the top layer, as damage was expected to occur in the matrix near the bottom θ-direction fibers first. Figure 4 shows an initial configuration of the two-ply and single-ply models.
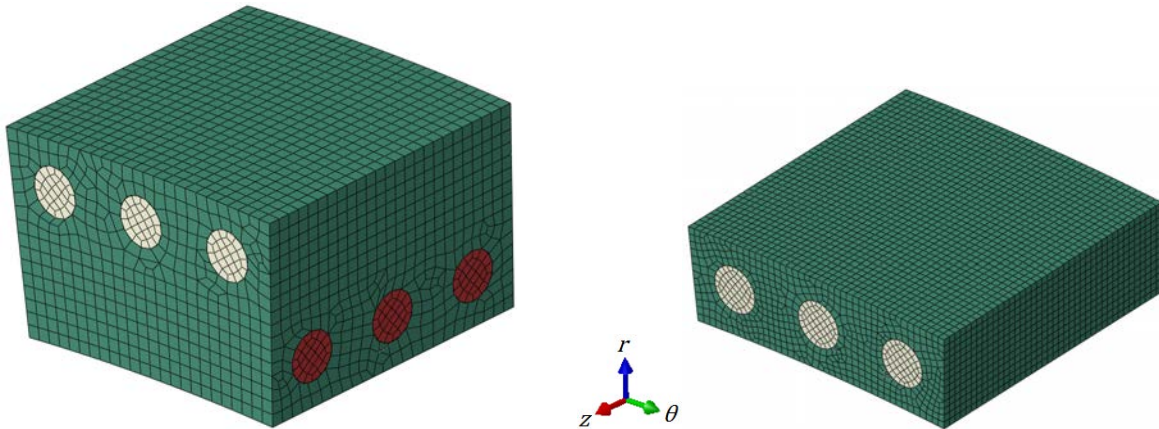

Figure 4. Two-Ply (Left) and One-Ply (Right) Finite-Element Model

The fibers were modeled as a linear elastic orthotropic material. Damage was incorporated into the fibers with a maximum principal stress condition. Above the maximum principal stress σ_{ps}, the fibers undergo fracture according to the described failure model. The matrix was modeled as an isotropic linear elastic material, with a similarly defined maximum principal stress failure criterion. Tables 2 and 3 show the material properties used for both the fiber and matrix.

Table 2. Constant Material Properties for the Fiber and Matrix

Property	E_{11} ksi (GPa)	E_{22} ksi (GPa)	E_{33} ksi (GPa)	G_{12} ksi (GPa)	G_{13} ksi (GPa)	G_{23} ksi (GPa)	v_{12}	v_{13}	v_{23}
Fiber	18500 (128)	1160 (8)	1160 (8)	435 (3)	435 (3)	667 (4.6)	0.28	0.28	0.46
Matrix	350 (2.4)	-	-	-	-	-	0.3	-	-

Table 3. Fracture Toughness Values for the Fiber and Matrix

Property	G_{IC} lb/in (N/m)	G_{IIC} lb/in (N/m)	G_{IIIC} lb/in (N/m)
Fiber	5 (875)	5 (875)	5 (875)
Matrix	5 (875)	5 (875)	5 (875)

Using XFEM enabled the modeling of fracture for both the fibers and the matrix. However, because the fibers were significantly stronger than the matrix, and because of the compressive stresses present, only the matrix was expected to fail. The interface between the matrix and fibers was modeled as a cohesive surface with a traction-separation damage law. The cohesion fails when the normal or shear stress reaches a maximum nominal stress $t_n^0(t_s^0, t_t^0)$. After damage initiation, the traction-separation law activates, giving a progressive damage that reaches full value at the specified displacement $\delta_n^f(\delta_s^f, \delta_t^f)$. Once a bond initially breaks, it will not reconnect with subsequent contact.

In order to investigate the effects of combining element fracture and cohesive failure into one model, the values for $t_n^0(t_s^0, t_t^0)$ were varied (see table 4). Cohesive strength is evaluated at $t_n^0(t_s^0, t_t^0)$ = 1, 5, 50, and 500 ksi. Maximum principal stress in the matrix required for crack forming was investigated at σ_{ps}^m = 0.5, 1, 5, and 10 ksi. A static analysis was conducted with external pressure as the loading condition.

Table 4. Fiber, Matrix, and Fiber/Matrix Cohesive Stress at Failure

Fiber σ_{ps}^f ksi (MPa)	Matrix σ_{ps}^m ksi (MPa)	Cohesive t_n^0, t_s^0, t_t^0 ksi (MPa)
250 (1723)	0.5, 1, 5, 10 (3.45, 6.9, 34.5, 69)	1, 5, 50, 500 (6.9, 34.5, 345, 3450)

RESULTS

Initially, the composite cylinder was simulated without fracture in the matrix or fibers and with a sufficiently high cohesive strength to prevent any cohesive damage from accumulating. Figure 5 shows the Von Mises and maximum principal stresses in the matrix alone. The highest Von Mises stress is seen between the axial fibers. As the cylinder is compressed, large compressive stresses are present in the circumferential θ-direction. With the fibers in the top ply aligned perpendicular to the highest stress direction, the surrounding matrix must support the load. As for the maximum principal stress, the inner section of the cylinder experiences the highest stress state, beneath the circumferential fibers. It is at this location that matrix cracking can be expected to form.
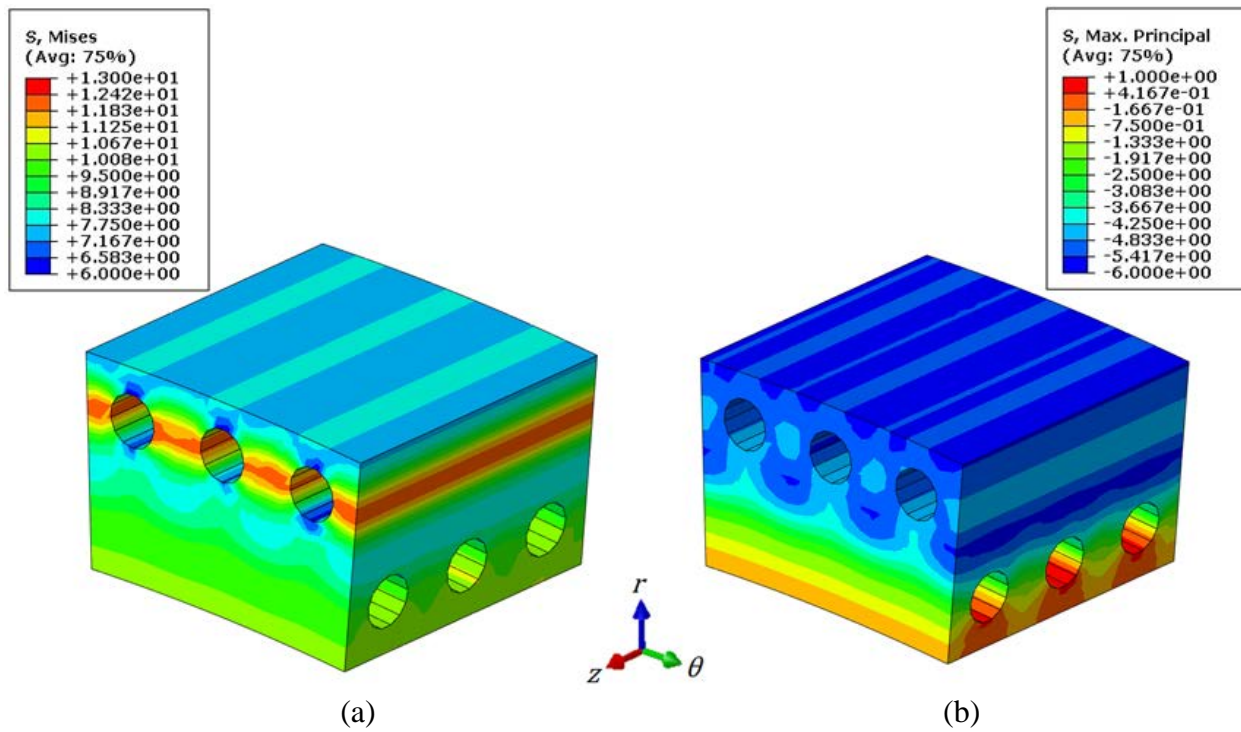

(a)   (b)

Figure 5. Stresses in Matrix Without Failure: (a) Von Mises and (b) Maximum Principal

The matrix is a candidate for future crack growth; the fibers are responsible for carrying the compressive load. Figure 6 shows the Von Mises and maximum principal stresses in the fibers. A significantly higher Von Mises stress state (figure 6(a)) can be seen in the circumferential fibers, which is attributed to the fact that the primary deformation is the decrease of the cylinder diameter. Though the axial fibers experience transverse compression, little load is supported in the fiber direction. It can be seen in figure 6(b) that the fibers in a maximum principal stress condition are, as expected, entirely in compression. Fracture, only occurring in tension, is not expected to be seen in the fibers.
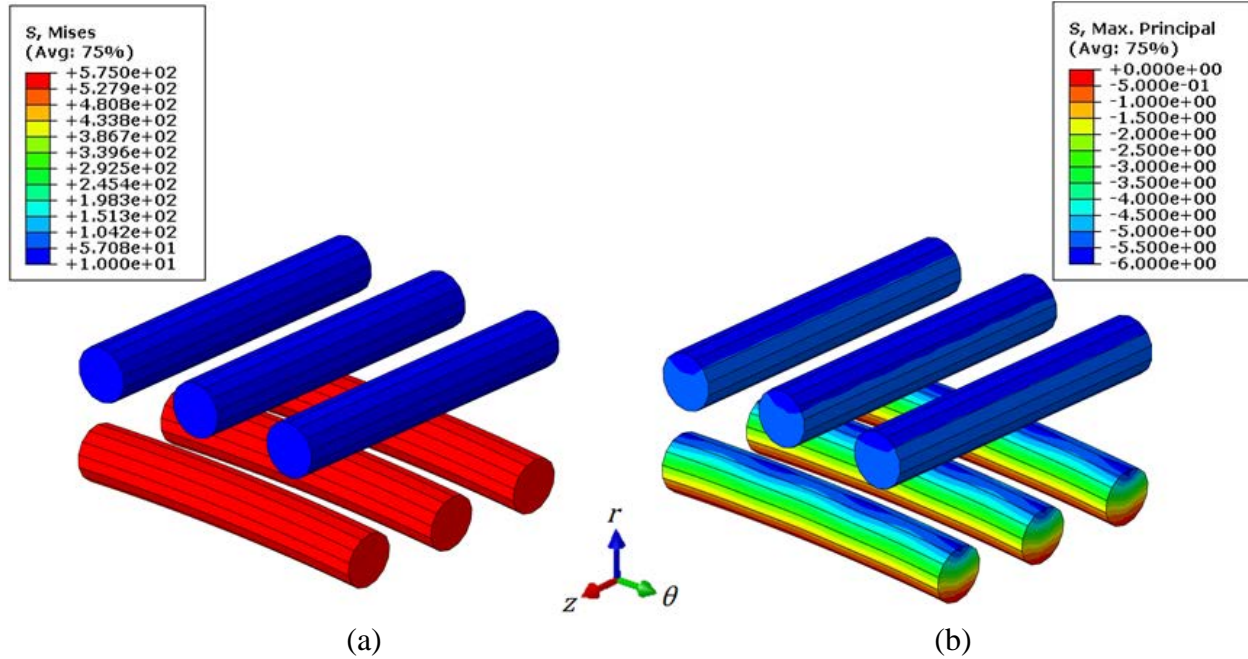

(a)   (b)

Figure 6. Stresses in Fibers Without Failure: (a) Von Mises and (b) Maximum Principal

In order for cracks to form and propagate in the matrix, the maximum principal stress must overcome σ_{ps}^m. In the interest of consistency, rather than change the external pressure p_e, σ_{ps}^m is reduced to induce failure. Figure 7 shows the translucent final configurations with $\sigma_{ps}^m = 0.5$, 1, 5, and 10 ksi, respectively. When fracture occurs, denoted in red, it is located near the bottom portion of the center circumferential fiber. Fracture initiates near multiple sites along the fiber, then propagates in the circumferential direction until reaching the boundaries. Presumably, because of the cylindrical boundary conditions applied to the model, fracture can occur near any fiber in the bottom layer. It is assumed that, after initial damage accumulation, the stress state is relaxed to a point where subsequent fracture sites are unlikely to form. At $\sigma_{ps}^m = 0.5$ ksi, the crack propagates along the entire length of the fiber. The crack initiates in multiple sites when $\sigma_{ps}^m = 1$ ksi but does not propagate fully. At $\sigma_{ps}^m = 5$, 10 ksi, the requisite failure criterion is not reached and no cracks are formed.
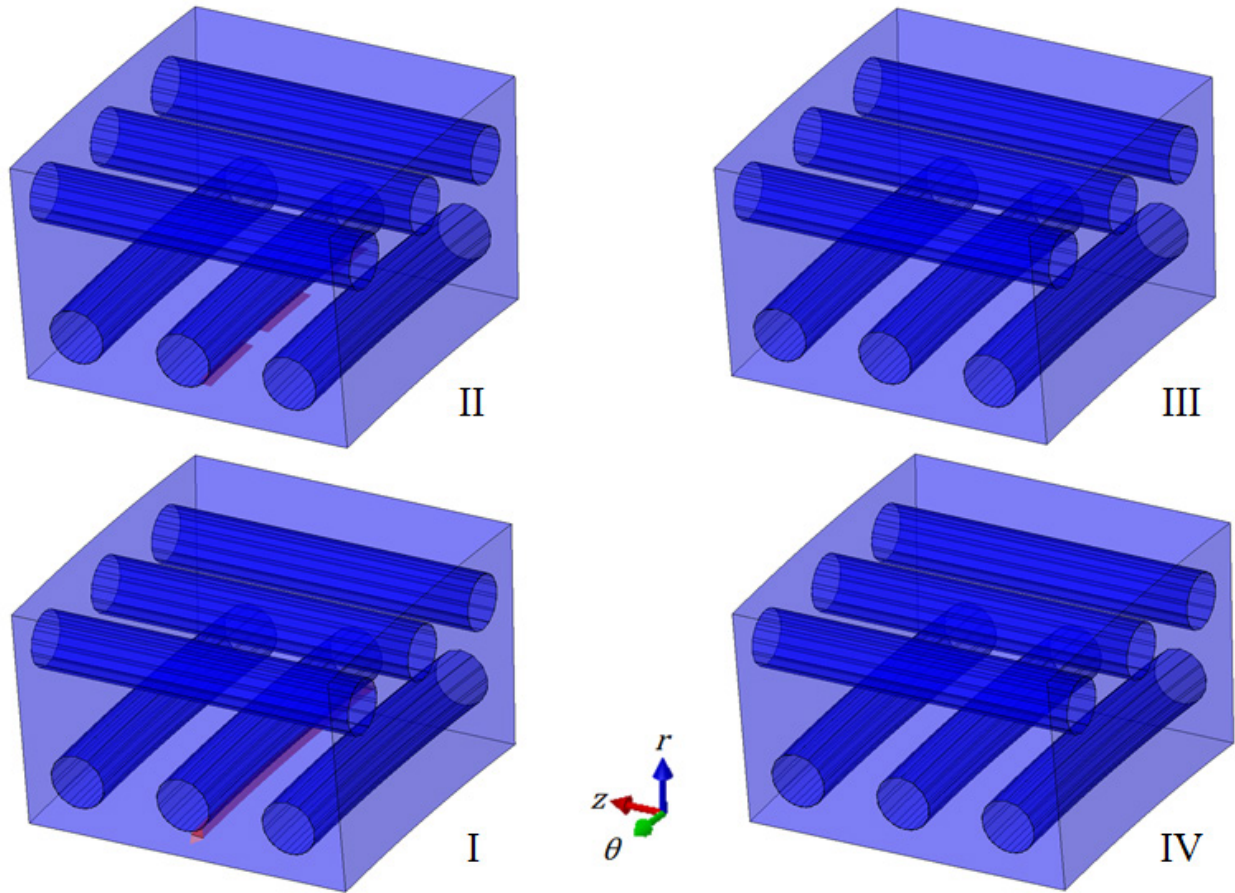

Figure 7. Crack Formation and Propagation in $\sigma_{ps} = 0.5$ ksi (I), 1 ksi (II), 5 ksi (III), and 10 ksi (IV)

To investigate the cohesive interface failure, σ_{ps}^m was maintained at 5 ksi, higher than the accumulated principal stress in the model. The required nominal stress to initiate cohesive failure was varied with $t_n^0(t_s^0, t_t^0) = 1, 5, 50$ and 500 ksi. Figure 8 shows the cohesive damage D for each of these analyses. At $t_n^0 = 1$ ksi, nearly the entire interface is severed. The majority of the interface was damaged with $t_n^0 = 5$ ksi, while damage occurred only in a few locations when $t_n^0 = 50$ ksi. As expected, no damage occurred when $t_n^0 = 500$ ksi. When only partial damage was present, the cohesive bonds initially failed at the diagonal regions of the cylindrical fibers.
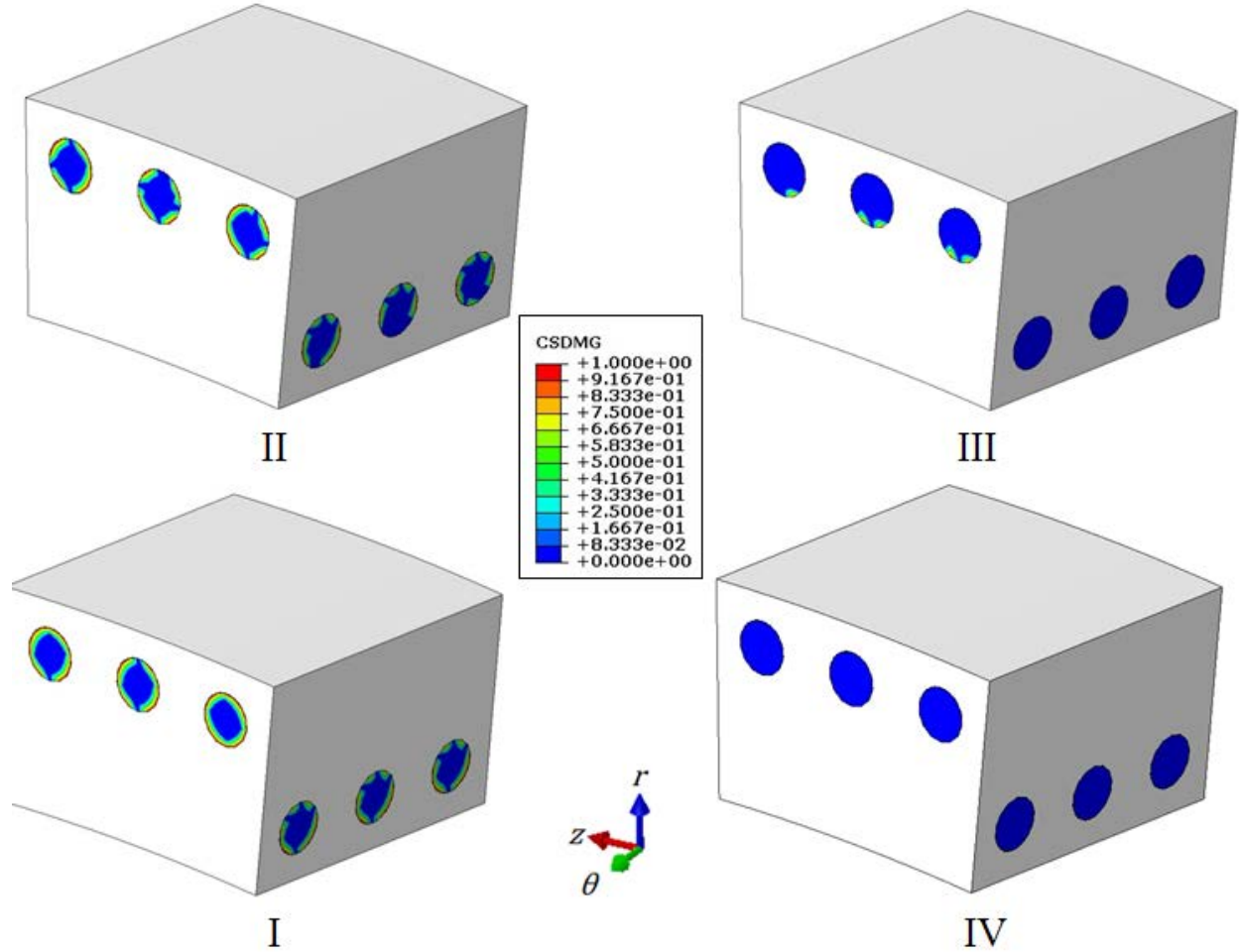

Figure 8. Cohesive Damage D with $t_n^0(t_s^0, t_t^0)$ = 1 ksi (I), 5 ksi (II), 50 ksi (III), and 500 ksi (IV) ksi

When cohesive interfacial damage was combined with matrix cracking, one can see multiple methods of material fracture in a single model. In order to properly assess the combination of these two failure phenomena, the matrix maximum principal stress prior to failure was $\sigma_{ps}^m = 1$ ksi and the cohesive interface maximum nominal stress was $t_n^0 = 5$ ksi. Figure 9 illustrates the Von Mises stress, interfacial damage *D,* and the crack location. Similar to the damage shown in figure 8, the fiber/matrix interface is partially broken around all fibers. A crack emerges along the center circumferential fiber and grows in the θ-direction.
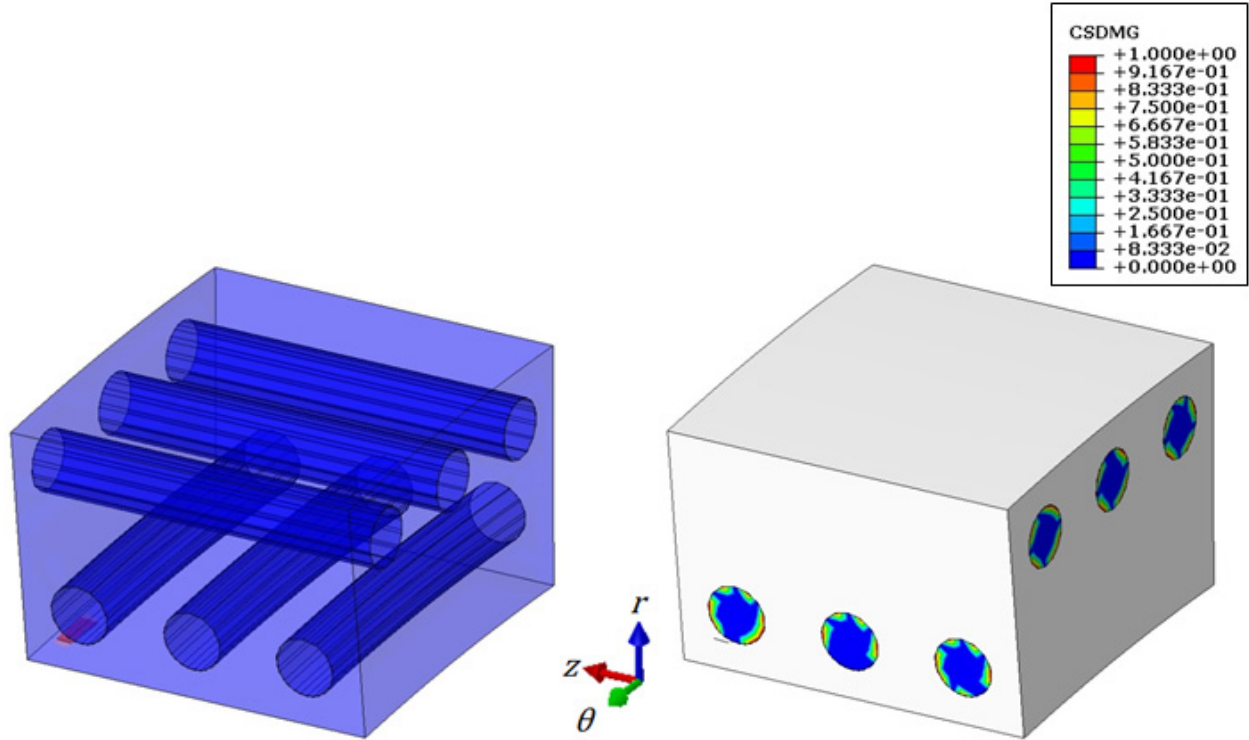

Figure 9. Cohesive Damage D and Crack Formation with $t_n^0(t_s^0, t_t^0)$ ***= 5 ksi and*** σ_{ps}^m ***= 1 ksi***

In the previous simulations, cracks formed and grew along the circumferential θ-direction fibers; moreover, these fibers experienced the highest stress. If the θ-direction fibers were removed, the structural capacity would be supported by the matrix and transverse compression of the z-direction fibers. When the circumferential fibers were removed, with just one ply of axial fibers in the cylinder, fracture occurred in the matrix along the direction of the fibers. This fracture, however, occurred at a significantly lower external pressure p_e = 1 ksi. Without the reinforcing circumferential fibers, the matrix undergoes more deformation and eventual failure. Furthermore, some crack propagation was observed in the matrix in the θ-direction. Along with the formation of a crack, the cohesive interface was more severely damaged. Figure 10 shows the failure at p_e = 1 ksi for a representative one-ply simulation.
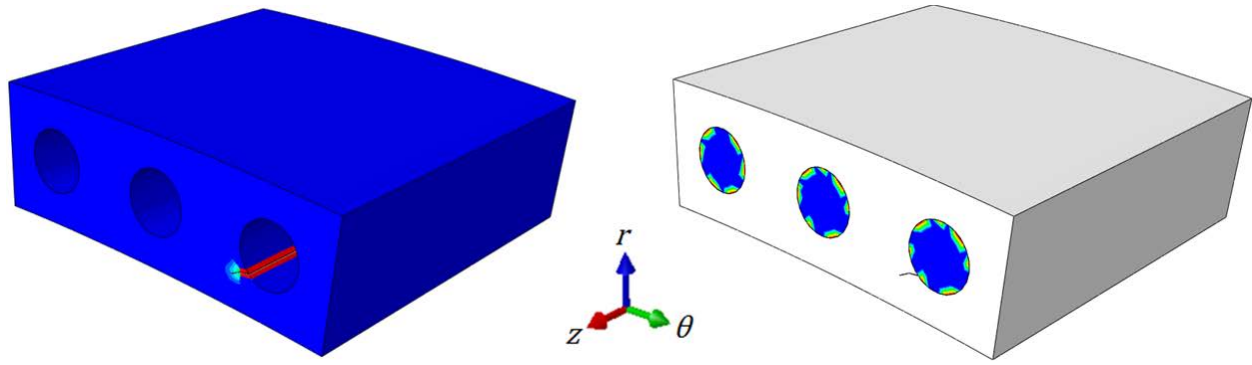

Figure 10. Cohesive Damage D and Crack Formation
with $t_n^0(t_s^0, t_t^0)$ = 50 ksi and σ_{ps}^m = 0.5 ksi

CONCLUSION

In this report, the application of the extended finite-element method (XFEM) to a 3-D finite-element model was combined with cohesive interface failure mechanisms to capture multiple methods of fracture in carbon fiber/epoxy composite cylinders. External pressure was used as a loading condition because typical applications of composite cylinders as underwater vessels are exposed to hydrostatic depth pressure. In the interest of consistency, geometry and pressure amplitude were held constant while material properties were modified. Thresholds for material failure prior to crack initiation were varied to determine failure thresholds for the given geometry and pressure loading. In order for fracture to occur in the matrix, the maximum principal stress was required to surpass the material property σ_{ps}^m. Fracture was not seen in the fibers because that stress condition was entirely compressive. At the lowest value of σ_{ps}^m, the crack initially formed near the circumferential θ-direction fibers, followed by propagation along the fiber direction. At higher σ_{ps}^m, only partial cracks formed, if at all.

In addition to modeling crack formation and growth, cohesive interface failure was investigated for varying cohesive strengths t_n^0. Complete cohesive failure occurred at the lowest t_n^0, and as t_n^0 increased, progressively less damage accumulated. When only partial damage was present, the cohesive bonds initially failed at the diagonal regions of the cylindrical fibers. Combining cohesive failure and material fracture allowed multiple damage mechanisms to be examined at once. Crack locations in the combined simulations were consistent with those that only included matrix fracture without cohesive failure behavior.

One-ply composite cylinders were analyzed as a means to isolate the influence of axial fibers on the structural capability of the composite cylinder without reinforcing circumferential fibers. For the one-ply simulations, fracture occurred at significantly lower external pressure p_e. Matrix fracture occurred similarly along the fibers but then propagated in the θ-direction. Considerable damage occurred along the fiber/matrix cohesive interface as well.

This research demonstrates the ability to model multiple modes of failure in composite materials using XFEM and cohesive interface failure—thus improving modeling efficacy, diminishing the need for build-test-build methodology, and vastly reducing cost and time requirements.

REFERENCES

1. P. Davies, L. Riou, F. Mazeas, P. Warnier, "Thermoplastic Composite Cylinders for Underwater Applications," *Journal of Thermoplastic Composite Materials*, vol. 18, no. 5, pp. 417-443, 2005.

2. P. B. Gning, M. Tarfaoui, F. Collombet, L. Riou, P. Davies, "Damage Development in Thick Composite Tubes Under Impact Loading and Influence on Implosion Pressure: Experimental Observations," *Composites Part B: Engineering*, vol. 36, pp. 306-318, 2005.

3. J. R. Tarpani, M. T. Milan, D. Spinelli, W.W. Bose, "Mechanical Performance of Carbon-Epoxy Laminates Part I: Quasi-Static and Impact Bending Properties," *Materials Research*, vol. 9, no. 2, pp. 115-120, 2005.

4. S. Kyriakides, R. Arseculeratne, E .J. Perry, K. M. Liechti, "On the Compressive Failure of Fiber Reinforced Composites," *International Journal of Solids Structures*, vol. 32, no. 6/7, pp. 689-738, 1995.

5. N. S. Choi, "Rate Effects on the Delamination Fracture of Multidirectional Carbon-Fiber/Epoxy Composites Under Mode I Loading," *Journal of Materials Science*, vol. 36, pp. 2257-2270, 2001.

6. G. C. Jacob, J. M. Starbuck, J. F. Fellers, S. Simunovic, R. G. Boeman, "Fracture Toughness in Random-Chopped Fiber-Reinforced Composites and Their Strain Rate Dependence," *Journal of Applied Polymer Science*, vol. 100, pp. 695-701, 2006.

7. K. L. Kepple, G. P. Sanborn, P. A. Lacasse, K. M. Gruenberg, W. J. Ready, "Improved Fracture Toughness of Carbon Fiber Composite Functionalized with Multi Walled Carbon Nanotubes," *Carbon*, vol. 46, pp. 2026-2033, 2008.

8. M. S. Prasad, C. S. Venkatesha, T. Jayaraju, "Experimental Methods of Determining Fracture Toughness of Fiber Reinforced Polymer Composites under Various Loading Conditions," *Journal of Minerals & Materials Characterization & Engineering*, vol. 10, no. 13, pp. 1263-1275, 2011.

9. L. Mishnaevsky Jr., P. Brøndsted, "Micromechanical Modeling of Damage and Fracture of Unidirectional Fiber Reinforced Composites: A Review," *Computational Materials Science*, vol. 44, no. 4, pp. 1351-1359, 2009.

10. S. T. Pinho, L. Iannucci, P. Robinson, "Physically-Based Failure Models and Criteria for Laminated Fibre-Reinforced Composites with Emphasis on Fibre Kinking: Part I: Development," *Composites Part A: Applied Science and Manufacturing*, vol. 37, no. 1, pp. 63-73, 2006.

REFERENCES (Cont'd)

11. H. Wang, Q. H. Qin, H. Zhou, H. Miao, "Damage Progress Simulation in Unidirectional Composites by Extended Finite Element Method (XFEM)," *Advanced Materials Research*, vol. 152 and 153, pp. 73-76, 2011.

12. R. Krueger, "The Virtual Crack Closure Technique: History, Approach and Applications," NASA/Contractor Report-2002-211628, National Institute of Aerospace, Hampton, VA 2002.

13. H. Sun, S. Rajendran, D. Q. Song, "Finite Element Analysis on Delamination Fracture Toughness of Composite Specimens," *Proceedings of 2nd Asian ANSYS User Conference*, Singapore, 1998.

14. H. S. M. Waseem, N. K. Kumar, "Finite Element Modeling for Delamination Analysis of Double Cantilever Beam Specimen," *SSRG International Journal of Mechanical Engineering*, vol. 1, no. 5, pp. 27-33, 2014.

15. P. P. Camanho, C. G. Dávila, D. R. Ambur, "Numerical Simulation of Delamination Growth in Composite Materials," NASA/TP-2001-211041, National Aeronautics and Space Administration, Hampton, VA, 2001.

16. W. Zhao, "Mode I Delamination Fracture Characterization of Polymeric Composites Under Elevated Temperature," Mechanical and Aerospace Engineering – Dissertations, Paper 59, Syracuse University, 2011.

17. G. Wimmer, C. Schuecker, H. E. Pettermann, "Numerical Simulation of Delamination Onset and Growth in Laminated Composites," Vienna University of Technology, Vienna, 2006.

18. D. Segala, P. V. Cavallaro, "Energy Absorption Mechanisms in Unidirectional Composites Subjected to Dynamic Loading Events," NUWC-NPT Technical Report 12,090, Naval Undersea Warfare Center Division Newport, RI, 30 March 2012.

19. D. Motamedi, A. S. Milani, "3D Nonlinear XFEM Simulation of Delamination in Unidirectional Composite Laminates: A Sensitivity Analysis of Modeling Parameters," *Open Journal of Composite Materials*, vol. 3, pp. 113-126, 2013.

20. M. Levén, D. Rickert, "Stationary 3D Crack Analysis with Abaqus XFEM for Integrity Assessment of Subsea Equipment," Chalmers University of Technology, Thesis 35, Göteborg, 2012.

21. D. M. Grogan, S. B. Leen, C. M. Ó Brádaigh, "An XFEM-Based Methodology for Fatigue Delamination and Permeability of Composites," *Composite Structures*, vol. 107, pp. 205-218, 2014.

22. E. Benvenuti, O. Vitarelli, A. Tralli, "Delamination of FRP-Reinforced Concrete by Means of an eXtended Finite Element Formulation," *Composites Part B: Engineering*, vol. 43, no. 8, pp. 3258-3269, 2012.

23. J. L. Curiel-Sosa, N. Karapurath, "Delamination Modelling of GLARE Using the Extended Finite Element Method," *Composites Science and Technology*, vol. 72, no. 7, pp. 788-791, 2012.

24. M. C. S. Moreno, J. L. Curiel-Sosa, J. Navarro-Zafra, J. L. Martinez Vicente, J. J. López Cela, "Crack Propagation in a Chopped Glass-Reinforced Composite under Biaxial Testing by Means of XFEM," *Composite Structures*, vol. 119, pp. 264-271, 2015.

25. D. Motamedi, "Nonlinear XFEM Modeling of Delamination in Fiber Reinforced Composites Considering Uncertain Fracture Properties and Effect of Fiber Bridging," PhD Dissertation, University of British Columbia, 2013.

26. T. Nagashima, H. Suemasu, "Stress Analyses of Composite Laminate with Delamination Using XFEM," *International Journal of Computational Methods*, vol. 3, no. 4, pp. 521, 2006.

27. M. Benzeggagh, M. Kenane, "Measurement of Mixed-Mode Delamination Fracture Toughness of Unidirectional Glass/Epoxy Composites with Mixed-Mode Bending Apparatus," *Composites Science and Technology*, vol. 56, pp. 439-449, 1996.

28. M. V. Gordić, I. M. Djordjević, D. R. Sekulić, Z. S. Petrović, M. M. Stevanović, "Delamination Strain Energy Release Rate in Carbon Fiber/epoxy Resin Composites," *Materials Science Forum*, vol. 555, pp. 515-519, 2007.

29. S. M. Lee, "An Edge Crack Torsion Method for Mode III Delamination Fracture Testing," *Journal of Composite Technology and Research*, vol. 15, no. 3, pp. 193-201, 1993.

30. T. Belytschko, T. Black, "Elastic Crack Growth in Finite Elements with Minimal Remeshing," *International Journal for Numerical Methods in Engineering*, vol. 45, pp. 601-620, 1999.

31. J. M. Melenk, I. Babuška, "The Partition of Unity Finite Element Method: Basic Theory and Applications," *Computer Methods in Applied Mechanics and Engineering*, vol. 39, pp. 289-314, 1996.

32. T. Belytschko, R. Gracie, G. Ventura, "A Review of Extended/Generalized Finite Element Methods for Material Modeling," *Modelling and Simulation in Materials Science and Engineering*, vol. 17, pp. 1-24, 2009.

INITIAL DISTRIBUTION LIST

Addressee	No. of Copies
Defense Technical Information Center	1
Center for Naval Analyses	1